PAPER • OPEN ACCESS

Suppressing the geometric dephasing of Berry phase by using modified dynamical decoupling sequences

To cite this article: Xiao-Ke Qin *et al* 2017 *New J. Phys.* **19** 013025

New Journal of Physics
The open access journal at the forefront of physics

Deutsche Physikalische Gesellschaft DPG
IOP Institute of Physics

Published in partnership with: Deutsche Physikalische Gesellschaft and the Institute of Physics

OPEN ACCESS

RECEIVED
30 September 2016

REVISED
26 November 2016

ACCEPTED FOR PUBLICATION
19 December 2016

PUBLISHED
20 January 2017

PAPER

Suppressing the geometric dephasing of Berry phase by using modified dynamical decoupling sequences

Xiao-Ke Qin[1,2], **Guang-Can Guo**[1,2] **and Zheng-Wei Zhou**[1,2]

[1] Key Laboratory of Quantum Information, University of Science and Technology of China, Chinese Academy of Sciences, Hefei, Anhui 230026, People's Republic of China
[2] Synergetic Innovation Center of Quantum Information and Quantum Physics, University of Science and Technology of China, Hefei, Anhui 230026, People's Republic of China

E-mail: zwzhou@ustc.edu.cn

Keywords: geometric dephasing, Berry phase, dynamical decoupling sequences

Abstract

Even though traditional dynamical decoupling methods have the ability to resist dynamic dephasing caused by low frequency noise, they are not appropriate for suppressing the residual geometric dephasing, which arises from the disturbance of the geometric loop in the parameter space. This prevents the precision of quantum manipulation-based geometric quantum gates from being promoted further. In this paper, we design two kinds of modified dynamical decoupling schemes to suppress the residual geometric dephasing. The further numerical simulation demonstrates the validity of our schemes.

1. Introduction

Berry phase [1] associated with the adiabatic evolution is a promising way to realize the precise control of quantum systems. By using spin echo (SE) methods [2] one can eliminate the dynamic phase included in the total phase [3] to realize the pure geometric quantum gate [4]. Up to now, nuclear magnetic-resonance (NMR) [5, 6], ultracold neutrons [7], graphene [8], superconducting circuit-QED [9, 10], etc have been used to study the Berry phase. The concept of geometric phase has been also generalized to the Aharonov–Anandan phase [11], non-unitary evolution [12], and mixed state [13].

In the field of quantum computation, decoherence induced by noise restricts the precision of quantum manipulation and the number of attainable quantum gates [14–17]. Quantum gates based on adjusting the Berry phase, ascribed to its geometric stability, are believed to have the ability to overcome certain kinds of random noise [18, 19]. However, recent studies exhibit that the adiabatic geometric phase gates are sensitive to noise in the control parameters [20, 21]. Although dynamical decoupling methods [22–24], used for adiabatic geometric phase gates, suppress the dynamic dephasing successfully, they do not work in resisting the geometric dephasing [21, 25], which comes from disturbance of the geometric loop in the parameter space. Suppressing the residual geometric dephasing becomes very vital in enhancing the accuracy of the quantum gates further.

In this paper, we reinvestigate a single qubit system driven by a slowly varying Hamiltonian. We simulate the classical fluctuation field along the z-axis using the Ornstein–Uhlenbeck (OU) process [24]. By analyzing the phase difference in the adiabatic evolution, we clarify the origin leading to the residual geometric dephasing. For instance, in the spin echo scheme, to eliminate the dynamic phase and to accumulate the Berry phase at the same time, the rotation directions of the magnetic field stay reversed before and after the flipping pulse is applied. This leads to the asymmetry of the parameters related to the low frequency noise. We design two new kinds of dynamical decoupling schemes to offset the asymmetry of noise coefficient and to suppress the residual geometric dephasing. The further numerical simulation demonstrates the validity of our schemes.

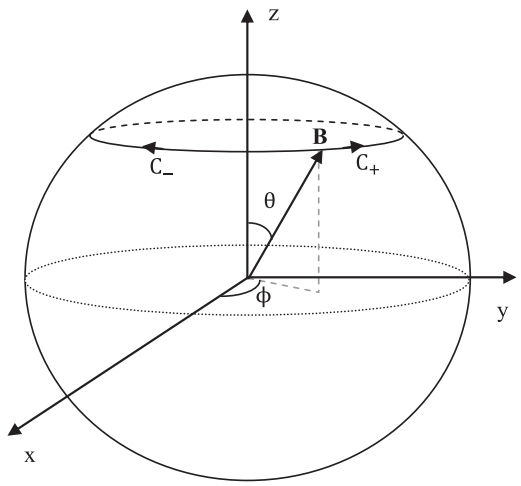

Figure 1. The controllable field $\boldsymbol{B}$, which varies along the closed anti-clockwise loop C_+ or the closed clockwise loop C_-.

2. Dephasing of the Berry phase

2.1. Berry phase

The qubit is driven by the Hamiltonian

$$H = \boldsymbol{B}(t) \cdot \boldsymbol{\sigma}/2. \tag{1}$$

Here, the controllable field $\boldsymbol{B}(t) = (B_1, B_2, B_3) = B_0(t)\mathbf{n}(t)$ and $\boldsymbol{\sigma} = (\sigma_x, \sigma_y, \sigma_z)$, where the unit direction vector $\mathbf{n}(t) = (\sin\theta\cos\phi, \sin\theta\sin\phi, \cos\theta)$. For simplicity, in this paper we set $\hbar = 1$. By using the unitary transformation $U(t) = \exp(\mathrm{i}\theta\sigma_y/2)\exp(\mathrm{i}\phi\sigma_z/2)\exp(\mathrm{i}\phi I/2)$, we obtain the Hamiltonian in the rotating frame [26, 27],

$$\bar{H} = U(t)HU^{\dagger}(t) + \mathrm{i}\dot{U}(t)U^{\dagger}(t) = \frac{1}{2}(\bar{\boldsymbol{B}} - \bar{\boldsymbol{\omega}}) \cdot \boldsymbol{\sigma} - \frac{1}{2}\dot{\phi}I, \tag{2}$$

where $\bar{\boldsymbol{B}} = (0, 0, B_0)$ and $\bar{\boldsymbol{\omega}} = (-\dot{\phi}\sin\theta, \dot{\theta}, \dot{\phi}\cos\theta)$. In the ideal situation, we assume that $\boldsymbol{B}(t)$ traverses the closed anti-clockwise(clockwise) loop $C_+(C_-)$ in the time T, where $B_0 = \text{const}$, $\theta = \text{const}$, and ϕ changes from 0 to $2m\pi$ with the integer winding number m as shown in figure 1. Under the uniform rotation, i.e. $\dot{\phi} = 2m\pi/T = \omega_{\mathrm{rf}}$, the adiabatic condition is $|\omega_{\mathrm{rf}}/B_0| \ll 1$ [21]. When $\boldsymbol{B}(t)$ does the anti-clockwise (clockwise) rotation about z-axis, $\omega_{\mathrm{rf}} > 0$ ($\omega_{\mathrm{rf}} < 0$). We expand $\Omega = |\bar{\boldsymbol{B}} - \bar{\boldsymbol{\omega}}|$ as follow

$$\begin{aligned}\Omega &= \sqrt{\left(B_0 - \omega_{\mathrm{rf}}\cos\theta\right)^2 + \omega_{\mathrm{rf}}^2\sin^2\theta} \\ &\approx B_0 - \omega_{\mathrm{rf}}\cos\theta + \frac{\omega_{\mathrm{rf}}^2\sin^2\theta}{2B_0} + o\left(\omega_{\mathrm{rf}}^2/B_0\right).\end{aligned} \tag{3}$$

After the time of duration T, the phases of the eigenstates of the Hamiltonian in equation (2) (with the eigenvalue ± 1) can be calculated as:

$$\begin{aligned}\gamma_{\pm}^0 &= \mp\frac{1}{2}\int_0^T \Omega\mathrm{d}t + \frac{1}{2}\int_0^T \omega_{\mathrm{rf}}\mathrm{d}t \\ &\approx \mp\frac{1}{2}B_0T + m\pi(1 \pm \cos\theta) \mp \frac{m\pi\omega_{\mathrm{rf}}}{2B_0}\sin^2\theta + \cdots.\end{aligned} \tag{4}$$

Here, the first term refers to the dynamic phase (proportional to T), the second one is the Berry phase (independent of T) and the third one is the non-adiabatic correction (proportional to $1/T$).

The Berry phase here also can be obtained in a natural frame. Because the intersection angle between the vector $\bar{\boldsymbol{B}}$ and $\bar{\boldsymbol{B}} - \bar{\boldsymbol{\omega}}$ satisfies $\delta = \arctan\frac{\omega_{\mathrm{rf}}\sin\theta}{B_0 - \omega_{\mathrm{rf}}\cos\theta} \approx 0$, in the rotating frame the eigenstates of the Hamiltonian in equation (2) can be approximated as $|\mathbf{n}_+\rangle = (1, 0)^T$ and $|\mathbf{n}_-\rangle = (0, -1)^T$. Here, $|\mathbf{n}_+\rangle$ and $|\mathbf{n}_-\rangle$ are the eigenstates of $\frac{1}{2}(\bar{\boldsymbol{B}} - \bar{\omega}_z) \cdot \boldsymbol{\sigma}$, and $\bar{\omega}_z$ refers to the z component of the vector $\bar{\boldsymbol{\omega}}$. Thus, in natural frame, the eigenstates of the operator $\mathbf{n}(t) \cdot \boldsymbol{\sigma}$ with the eigenvalue $s = \pm 1$ can be written as:

$$|\psi_{+1}(\boldsymbol{B}(t))\rangle = U^{\dagger}(t)|\mathbf{n}_{+}\rangle = \begin{pmatrix} \mathrm{e}^{-\mathrm{i}\phi}\cos\frac{\theta}{2} \\ \sin\frac{\theta}{2} \end{pmatrix}, \tag{5a}$$

$$|\psi_{-1}(\boldsymbol{B}(t))\rangle = U^{\dagger}(t)|\mathbf{n}_{-}\rangle = \begin{pmatrix} \mathrm{e}^{-\mathrm{i}\phi}\sin\frac{\theta}{2} \\ -\cos\frac{\theta}{2} \end{pmatrix}. \tag{5b}$$

Berry phase can be represented as [3, 21]

$$\gamma_{\pm}^{\mathrm{g}} = \mathrm{i}\oint_{C}\langle\psi_{\pm1}(\boldsymbol{B})|\nabla_{B}|\psi_{\pm1}(\boldsymbol{B})\rangle\,\mathrm{d}\boldsymbol{B} = m\pi(1\pm\cos\theta). \tag{6}$$

2.2. Observation of the Berry phase

To observe the Berry phase, it is necessary to induce the interference between two relevant phases. In the natural frame, assume that the initial superposition state $|\psi(0)\rangle = 1/\sqrt{2}\sum_{s=\pm1}|\psi_{s}(\boldsymbol{B}(0))\rangle$ adiabatically evolutes to the final state $|\psi(T)\rangle = 1/\sqrt{2}\sum_{s=\pm1}\mathrm{e}^{\mathrm{i}\gamma_{s}}|\psi_{s}(\boldsymbol{B}(0))\rangle$. Here, the phase difference $\gamma = \gamma_{-1} - \gamma_{+1}$ is the physical observable, which contains the contributions from the dynamic phase, Berry phase and the other corrections. To observe the phase difference caused by the Berry phase, ones usually take advantage of the SE technique [2, 4, 5, 7, 9] to eliminate the part of the dynamic phase (here, we omit the correction term). For instance, to obtain the phase difference of the Berry phase for the close anti-clockwise loop C_{+} ($m = 2$), ones first adiabatically drives the Hamiltonian H to vary along the anti-clockwise loop C_{+} ($m = 1$), next, a π pulse is added to swap the eigenstates of the Hamiltonian H, then, an adiabatic evolution along the clockwise loop C_{-} ($m = -1$) is applied, finally, a π pulse is used again to swap the eigenstates of the Hamiltonian H. In this process, by virtue of the swapping of eigenstates, the dynamic phase is offset. Thus $\gamma_{\pm1} = \gamma_{\pm}^{0}(m = 1) + \gamma_{\mp}^{0}(m = -1) = \pm 2\pi\cos\theta$. The observable phase difference $\gamma = \gamma_{-1} - \gamma_{+1} = \gamma_{-}^{\mathrm{g}} - \gamma_{+}^{\mathrm{g}} = -4\pi\cos\theta$ is pure geometric.

Based on the above protocol, we find that the final phase γ_{s} is the accumulation of the phases from segmented adiabatic evolution. For the convenience of the following context we rewrite the phase $\gamma_{s}(s = \pm 1)$ as:

$$\gamma_{s} = \sum_{k}\gamma_{s_k}^{k}\left(C_{l_k}^{\theta_k,s_k}\right). \tag{7}$$

Here, the total evolution time T is divided into n segements: $T = \sum_{k=1}^{n}\int_{T_{k-1}}^{T_k}\mathrm{d}t$ where the adjacent time intervals are separated by the swapping pulse and $s = s_k$ ($s = -s_k$) for the odd (even) k. $\gamma_{s_k}^{k}(C_{l_k}^{\theta_k,s_k})$ is the phase integral for the eigenstate of the operator $\mathbf{n}(t)\cdot\boldsymbol{\sigma}$ with the eigenvalue s_k in the kth time interval $[T_{k-1},\ T_k]$ and $C_{l_k}^{\theta_k,s_k}$ refers to the trajectory of the vector $s_k\mathbf{n}(t)$ in the Bloch sphere, θ^{k} is the intersection angle between the vector $\mathbf{n}(t)$ and z-axis in the kth time interval.

$$\gamma_{s_k}^{k}\left(C_{l_k}^{\theta_k,s_k}\right) = -\frac{s_k}{2}\int_{T_{k-1}}^{T_k}\Omega\mathrm{d}t + \pi l_k, \tag{8}$$

where $l_k = \omega_{\mathrm{rf}}^{k}(T_k - T_{k-1})/2\pi$, ω_{rf}^{k} is the circular frequency in the kth trajectory $C_{l_k}^{\theta_k,s_k}$ and $\omega_{\mathrm{rf}}^{k} > 0(\omega_{\mathrm{rf}}^{k} < 0)$ refers to the anti-clockwise (clockwise) rotation about the z-axis.

2.3. Dephasing due to the low-frequency classical fluctuating field

Consider the classical fluctuating field $\boldsymbol{K}(t) = (K_1, K_2, K_3)$, where K_i, $(i = 1, 2, 3)$ is the statistical variable. The total Hamiltonian of the qubit can be written as $H_T = \boldsymbol{B}_T(t)\cdot\boldsymbol{\sigma}/2$ with $\boldsymbol{B}_T(t) = \boldsymbol{B}(t) + \boldsymbol{K}(t)$. For simplicity, we follow the same assumption in [4, 7, 26, 27] $\boldsymbol{K}(t) = (0, 0, K_3)$, which is named the K_3 noise and independent of the controllable field $\boldsymbol{B}(t)$. For K_3 noise as OU processes [24] with a Lorentzian spectrum of bandwidth Γ_3 and the noise power α_3, it follows that

$$L_3(\tau) = \langle K_3(t+\tau)K_3(t)\rangle = \alpha_3\mathrm{e}^{-\Gamma_3|\tau|}, \tag{9}$$

which produces the power spectrum

$$S_3(\omega) = 2\alpha_3\Gamma_3/(\Gamma_3^2 + \omega^2). \tag{10}$$

Here, we assume that the noise bandwidth Γ_3 is much smaller than B_0, which prevents the incoherent transition between two eigenstates.

Due to the existence of the classical fluctuating field, as far as the Hamiltonian in the rotating frame is concerned, it will be revised by replacing $\bar{\mathbf{B}}$ by $\bar{\mathbf{B}}_T = (-K_3\sin\theta,\ 0,\ B_0 + K_3\cos\theta)$. Thereby, we may also obtain the expansion of $\Omega_T = |\bar{\boldsymbol{B}}_T - \bar{\boldsymbol{\omega}}|$,

$$\Omega_T = \left[\left(B_0 - \omega_{\rm rf}\cos\theta + K_3\cos\theta\right)^2 + \left(\omega_{\rm rf} - K_3\right)^2\sin^2\theta\right]^{\frac{1}{2}}$$
$$\approx \Omega + \cos\theta K_3 - \frac{\omega_{\rm rf}\sin^2\theta}{B_0}K_3 + o(K_3^2/B_0), \tag{11}$$

where the coefficients $\cos\theta$ and $-\omega_{\rm rf}\sin^2\theta/B_0$ originate from the disturbances of the dynamic phase and the Berry phase, respectively.

When $|K_3(t)| \ll B_0$ and $|\omega_{\rm rf}| \ll B_0$, the vector $\bar{B}_T - \bar{\omega}$ is approximate along the same direction with the vector $\bar{B}$. Since there is the classical fluctuation field the phase difference γ produces a statistical distribution, which causes the dephasing [21]. In equation (11), if we only consider the linear terms of K_3, the nondiagonal element $\rho_{-1,1}(T)$ in the final density matrix has the form:

$$\rho_{-1,1}(T) = W e^{i\langle\gamma\rangle}\rho_{-1,1}(0) \tag{12}$$

with the coherence function [28]

$$W = \langle e^{i\varphi}\rangle = e^{-\langle\varphi^2\rangle/2}, \tag{13}$$

where

$$\varphi = -\sum_{k=1}^{n}\int_{T_{k-1}}^{T_k} s_k(\cos\theta - \omega_{\rm rf}^k\sin^2\theta/B_0)K_3(t)\,dt \tag{14}$$

with $s_1 = -1$. Generally, the coefficient $s_k(\cos\theta - \omega_{\rm rf}^k\sin^2\theta/B_0)$ in the adiabatic trajectory $C_{l_k}^{\theta_k,s_k}$ is unchanged. The term related to the coefficient $s_k\cos\theta$ gives rise to the dynamic dephasing (disturbance of $|B_T|$), and the one related to the coefficient $-s_k\omega_{\rm rf}^k\sin^2\theta/B_0$ induces geometric dephasing [4, 21]. We define $\chi = -\ln W = \langle\varphi^2\rangle/2$ to characterize the dephasing rate. For simplicity, we assume the Bloch vector keeps the same rate of rotation $\omega_B = |\omega_{\rm rf}^k|$ in the different trajectory $C_{l_k}^{\theta_k,s_k}$.

In the following context, we set the whole time of duration $T = 4\pi/\omega_B$ all the time. For free induction decay (FID) (without any of a swapping pulse), by using the correlation function in equation (9), we obtain the dephasing rate in the case of the low-frequency noise $\Gamma_3 T \ll 1$

$$\chi \approx \left(\cos^2\theta - \frac{2\omega_B\cos\theta\sin^2\theta}{B_0} + \frac{\omega_B^2\sin^4\theta}{B_0^2}\right)\frac{\alpha_3 T^2}{2}. \tag{15}$$

Under the adiabatic approximation, equation (15) can be further reduced to:

$$\chi = \cos^2\theta\frac{\alpha_3 T^2}{2}, \tag{16}$$

which is same as the dynamic dephasing of the qubit with time-independent Hamiltonian ($\theta = 0$).

3. Schemes suppressing geometric dephasing

3.1. Residual geometric dephasing

The dynamical decoupling method can be usually used to suppress the low-frequency noise, which inspires its application for the Berry phase (see the appendix). In this subsection, we will investigate the variation on dephasing rate χ by exerting traditional dynamical decoupling pulses. First, let us review the SE method, which is always used to cancel the dynamic phase and suppress the dynamic dephasing [4, 7, 24]. Assume that there is not any environmental noise, for the eigenstate $|\psi_{\pm1}(B(t))\rangle$ of the Hamiltonian H, the trajectory $C_{l_1=1}^{\theta,-1}C_{l_2=-1}^{\theta,+1}$ of its Bloch vector with the initial condition $\mathbf{b}(\mathbf{0}) = -\mathbf{n}(0)$ is exhibited in figure 2(a). (For simplicity, in the following all figures on the trajectory of the Bloch vector $-\mathbf{n}(0)$ will act as the starting point of the adiabatic trajectory.) As a result, for the superposition state $|\psi(t)\rangle = 1/\sqrt{2}\sum_{s=\pm1}|\psi_s(B(t))\rangle$ (as shown in section 2.2) the dynamic phase is canceled and the Berry phase difference is accumulated, i.e. $\langle\gamma\rangle = -4\pi\cos\theta$.

When the classical fluctuating field is induced, by using equation (13) and the correlation function in equation (9), we derive out

$$\chi = \frac{\alpha_3}{\Gamma_3^2}\cos^2\theta\left(\Gamma_3 T - 3 + 4e^{-\Gamma_3 T/2} - e^{-\Gamma_3 T}\right) + \frac{\alpha_3}{\Gamma_3^2}\frac{\omega_B^2\sin^4\theta}{B_0^2}\left(\Gamma_3 T - 1 + e^{-\Gamma_3 T}\right). \tag{17}$$

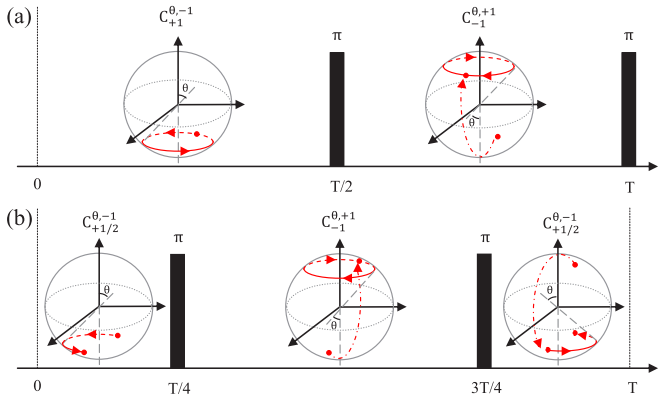

Figure 2. Trajectory of the Bloch vector $\mathbf{b}(t)$ with the initial condition $\mathbf{b}(0) = -\mathbf{n}(0)$ as one of the eigenstate of the transient Hamiltonian H in equation (1). The start point and end point of the trajectory segment are depicted by the red dots. Trajectories in (a) and (b) refer to $C_{+1}^{\theta,-1}C_{-1}^{\theta,+1}$ and $C_{+1/2}^{\theta,-1}C_{-1}^{\theta,+1}C_{+1/2}^{\theta,-1}$, respectively.

For the low-frequency noise with $\Gamma_3 T \ll 1$, we simplify the above equation as

$$\chi = \cos^2\theta\frac{\alpha_3\Gamma_3 T^3}{12} + \frac{\omega_B^2\sin^4\theta}{B_0^2}\frac{\alpha_3 T^2}{2}, \tag{18}$$

where the first term as the dynamic dephasing is far less than equation (16) and the second term represents the geometric dephasing [4, 21, 25]. It's obvious that SE suppresses the dynamic dephasing successfully. However, the geometric dephasing rate, which acts as one of higher order correction in equation (15), can not be suppressed by SE pulses. The residual geometric dephasing becomes dominant when $\frac{\cos^2\theta}{\sin^4\theta}\frac{\beta\kappa^2}{6} \ll 1$ with $\beta = \Gamma_3 T$ (timescale of the noise) and $\kappa = B_0/\omega_B$ (adiabaticity of the evolution). The geometric dephasing does not change with ω_B or T due to $\omega_B T = 4\pi$. Therefore, it is not able to be suppressed by the more adiabaticity (increasing T), which only increases the first term.

For the more higher-order dynamical decoupling sequences, such as Carr–Purcell–Meiboom–Gill [22] (CPMG) sequences, which trajectory on the Bloch vector is depicted by $C_{l_1=1/2}^{\theta,-1}C_{l_2=-1}^{\theta,+1}C_{l_3=1/2}^{\theta,-1}$ (see figure 2(b)), we may also obtain the dephasing rate as follows:

$$\chi = \cos^2\theta\frac{\alpha_3\Gamma_3 T^3}{48} + \frac{\omega_B^2\sin^4\theta}{B_0^2}\frac{\alpha_3 T^2}{2}. \tag{19}$$

Here, although dynamic dephasing rate is further suppressed, the geometric dephasing rate is the same as that of SE.

3.2. Modified dynamical decoupling sequences

To clarify why the geometric dephasing can not be further suppressed, let us look at the trajectory $C_{l_1=1}^{\theta,-1}C_{l_2=-1}^{\theta,+1}$ of the Bloch vector in SE scheme once again. Here, to eliminate the dynamical phase and to reserve the nonzero geometric phase at the same time, one has to keep $\omega_{\mathrm{rf}}^1 = -\omega_{\mathrm{rf}}^2$. This makes the coefficients $\cos\theta - \omega_{\mathrm{rf}}^1\sin^2\theta/B_0 \neq \cos\theta - \omega_{\mathrm{rf}}^2\sin^2\theta/B_0$ in the integral of equation (14). Therefore, under the low-frequency noise approximation, although $s_1 = -s_2$, the integrals in the path $C_{l_1=1}^{\theta,-1}$ and $C_{l_2=-1}^{\theta,+1}$ in the equation (14) can not be canceled out, which causes the residual geometric dephasing. The similar analysis is also appropriate for the CPMG scheme.

To further reduce the geometric dephasing dominated by the low-frequency noise, a fundamental starting point relies on how to make the integral items in equation (14) offset. Here, we provide out two kinds of schemes to suppress the residual geometric dephasing as follows.

Scheme 1: In this scheme, we vary the slant angle θ in the neighboring adiabatic path. By setting $\theta_1 = \theta^a$ and $\theta_2 = \theta^c$ and make the following equation hold:

$$\cos\theta^a - \frac{\omega_B\sin^2\theta^a}{B_0} = \cos\theta^c + \frac{\omega_B\sin^2\theta^c}{B_0}. \tag{20}$$

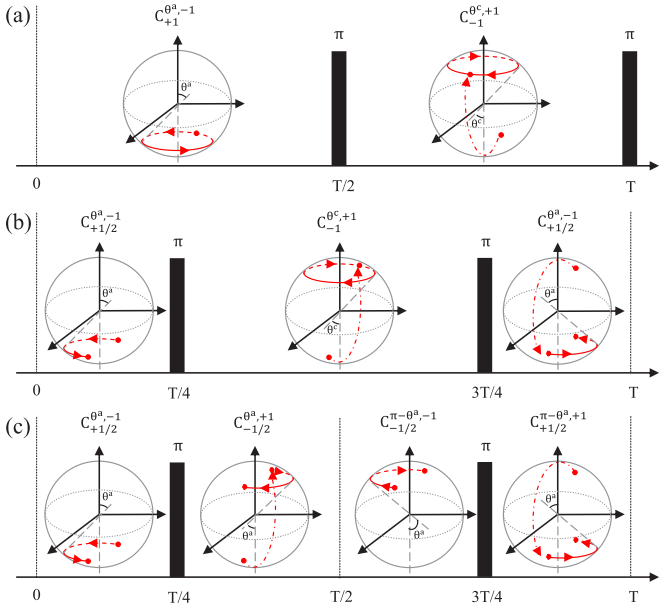

Figure 3. Trajectory of the Bloch vector $\mathbf{b}(t)$ with the initial condition $\mathbf{b}(0) = -\mathbf{n}(0)$. The start point and end point of the trajectory segment are represented by the red dots. The trajectories $C_{+1}^{\theta^a,-1}C_{-1}^{\theta^c,+1}$, $C_{+1/2}^{\theta^a,-1}C_{-1}^{\theta^c,+1}C_{+1/2}^{\theta^a,-1}$, and $C_{+1/2}^{\theta^a,-1}C_{-1/2}^{\theta^a,+1}C_{-1/2}^{\pi-\theta^a,-1}C_{+1/2}^{\pi-\theta^a,+1}$ are depicted by (a), (b), and (c) respectively.

Here, $\omega_B = \omega_{\rm rf}^1 = -\omega_{\rm rf}^2$. Under the adiabatic condition, we derive out the approximation solution,

$$\cos\theta^c = \frac{\cos\theta^a - \dfrac{2\omega_B}{B_0} + \dfrac{\omega_B^2\cos\theta^a}{B_0^2+\omega_B^2}}{1 + \dfrac{\omega_B^2 - 2\omega_B B_0\cos\theta^a}{B_0^2+\omega_B^2}}. \tag{21}$$

Therefore, we may modify the SE (CPMG) sequences as $C_{+1}^{\theta^a,-1}C_{-1}^{\theta^c,+1}$ ($C_{+1/2}^{\theta^a,-1}C_{-1}^{\theta^c,+1}C_{+1/2}^{\theta^a,-1}$). The trajectories of the corresponding Bloch vector $\mathbf{b}(t)$ are shown in figures 3(a) and (b), respectively.

Since there are different slant angles for two adjacent adiabatic paths, the final average Berry phase depends on two angles, i.e. $\langle\gamma\rangle = -2\pi(\cos\theta^a + \cos\theta^c)$. By using the modified scheme, we suppress the dephasing rate as

$$\chi = \left(\cos\theta^a - \frac{\omega_B\sin^2\theta^a}{B_0}\right)^2\frac{\alpha_3\Gamma_3T^3}{12}\begin{cases}1 & \text{SE}\\ 1/4 & \text{CPMG.}\end{cases} \tag{22}$$

For the low-frequency noise with $\Gamma_3 T \ll 1$, it decreases rapidly.

Scheme 2: To ensure geometric phase difference $\langle\gamma\rangle = -4\pi\cos\theta^a$ we may also devise a bit complicated adiabatic paths separated by swapping pulses: $C_{+1/2}^{\theta^a,-1}C_{-1/2}^{\theta^a,+1}C_{-1/2}^{\pi-\theta^a,-1}C_{+1/2}^{\pi-\theta^a,+1}$. In these paths, the coefficients of the integral in equation (14) are exhibited as follows:

$$\cos\theta^a - \frac{\omega_B\sin^2\theta^a}{B_0} \to -\cos\theta^a - \frac{\omega_B\sin^2\theta^a}{B_0} \to -\cos\theta^a + \frac{\omega_B\sin^2\theta^a}{B_0} \to \cos\theta^a + \frac{\omega_B\sin^2\theta^a}{B_0}, \tag{23}$$

Finally, all the items are offset and the dephasing rate becomes:

$$\chi = \cos^2\theta^a\frac{\alpha_3\Gamma_3T^3}{48} + \frac{\omega_B^2\sin^4\theta^a}{B_0^2}\frac{\alpha_3\Gamma_3T^3}{12}. \tag{24}$$

It means that the geometric dephasing is decreased by the factor $\Gamma_3 T/6$ than equations (18) and (19). The trajectories of the corresponding Bloch vector $\mathbf{b}(t)$ are shown in figure 3(c).

4. Numerical simulations

In this section we numerically simulate the classical fluctuating field to check the validity for the aforementioned analytical results. We divide the total time T into M intervals and keep $K_3(t)$ unchanged in every interval, where M is set large enough so that the time step Δt is far less than the correlation time $1/\Gamma_3$ of the classical fluctuation

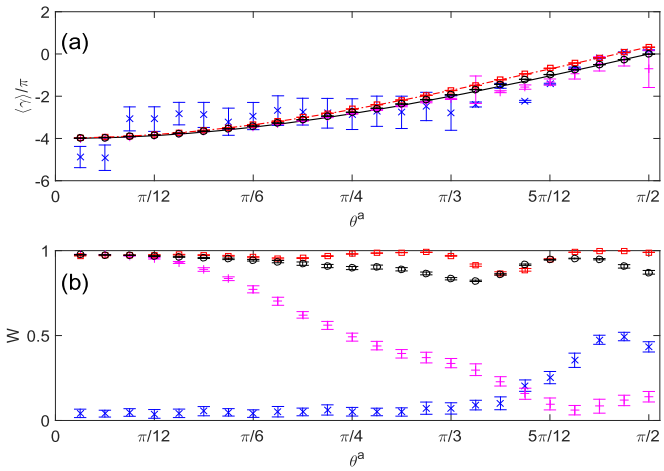

Figure 4. Numerical results under the various sequences: $C_{+2}^{\theta^a,-1}$ (blue cross), $C_{+1/2}^{\theta^a,-1}C_{-1}^{\theta^a,+1}C_{+1/2}^{\theta^a,-1}$ (magenta plus), $C_{+1/2}^{\theta^a,-1}C_{-1}^{\theta^c,+1}C_{+1/2}^{\theta^a,-1}$ (red square) and $C_{+1/2}^{\theta^a,-1}C_{-1/2}^{\theta^a,+1}C_{-1/2}^{\pi-\theta^a,-1}C_{+1/2}^{\pi-\theta^a,+1}$ (black circle). (a) The phase difference $\langle\gamma\rangle$ versus θ^a, where the theoretical Berry phase difference $-4\pi\cos\theta^a$ and $-2\pi\cos\theta^a-2\pi\cos\theta^c$ are described by the solid line and dot-dashed line, respectively; (b) Coherence function W versus θ^a. The error bars indicate the standard deviation.

field. We generate the random noise by using the method in the [29, 30]

$$K_3(t+\Delta t)=K_3(t)\mathrm{e}^{-\Gamma_3\Delta t}+K_3^{Rn}\sqrt{1-\mathrm{e}^{-2\Gamma_3\Delta t}}, \tag{25}$$

where K_3^{Rn} is a Gaussian distributed pseudo-random variable with the expectation $\langle K_3^{Rn}\rangle=0$ and the variance $\langle(K_3^{Rn})^2\rangle=\alpha_3$. The initial condition is determined by $K_3(0)=K_3^{Rn}$.

To satisfy the adiabatic approximation we take $B_0/\omega_B=12$, where $B_0=2\pi\nu$ and $\nu=100$ MHz. Meanwhile, considering the low-frequency noise limit $\Gamma_3/B_0\ll 1$, we set $\Delta t=(2\pi/B_0)/10$ as the minimum time scale. We also set $\Gamma_3=\beta/T$ and the variance of the classical fluctuation field $\alpha=\eta/\Gamma_3T^3$, where β and η are dimensionless parameters.

We start with the initial condition $|\psi(0)\rangle$ and numerically simulate the evolution of quantum state under classical fluctuating field. We repeat the calculation procedure 400 times until the average of the final density matrix ($\langle\rho(T)\rangle$) is convergent. The observable phase difference and coherence are given by $\langle\gamma\rangle=\arg\langle\rho_{-1,1}(T)\rangle$ and $W=|\langle\rho_{-1,1}(T)\rangle|/|\rho_{-1,1}(0)|$, respectively.

4.1. Results on different decoupling schemes

Under low frequency noise, we simulate the evolutions of quantum systems for different decoupling schemes characterized by the trajectories $C_{+2}^{\theta^a,-1}$, $C_{+1/2}^{\theta^a,-1}C_{-1}^{\theta^a,+1}C_{+1/2}^{\theta^a,-1}$, $C_{+1/2}^{\theta^a,-1}C_{-1}^{\theta^c,+1}C_{+1/2}^{\theta^a,-1}$ and $C_{+1/2}^{\theta^a,-1}C_{-1/2}^{\theta^a,+1}C_{-1/2}^{\pi-\theta^a,-1}C_{+1/2}^{\pi-\theta^a,+1}$. Here, we set $\beta=0.001$ and $\eta=400\beta$. The phase difference $\langle\gamma\rangle$ for different decoupling schemes are displayed in figure 4(a), where the theoretical Berry phase differences $-4\pi\cos\theta^a$ and $-2\pi\cos\theta^a-2\pi\cos\theta^c$ are described by the solid line and dot-dashed line, respectively. Figure 4(b) exhibits different coherence functions W versus θ^a. For CPMG scheme characterized by $C_{+1/2}^{\theta^a,-1}C_{-1}^{\theta^a,+1}C_{+1/2}^{\theta^a,-1}$, the coherence function W decays as θ^a grows. It is because the residual geometric dephasing becomes dominant when $|\sin\theta^a|$ increases. While, for the modified decoupling schemes, both $C_{+1/2}^{\theta^a,-1}C_{-1}^{\theta^c,+1}C_{+1/2}^{\theta^a,-1}$ and $C_{+1/2}^{\theta^a,-1}C_{-1/2}^{\theta^a,+1}C_{-1/2}^{\pi-\theta^a,-1}C_{+1/2}^{\pi-\theta^a,+1}$ suppress the geometric dephasing successfully, which improve the coherence and recover the Berry phases at the whole angle range.

It is slightly strange that the coherence for FID scheme is better than that for CPMG in large θ. The reason is that CPMG scheme makes the second term in equation (15) disappear which originally resists the residual geometric dephasing.

4.2. The correlation time

We also investigate the suppressing performance of various decoupling schemes versus the correlation time of the low-frequency fluctuating field. Here, we fix the angle $\theta^a=5\pi/12$. By keeping the total evolution time T unchanged we may use $\beta=\Gamma_3T$ to adjust the correlation time of K_3, where $\beta\in[0.005,\ 5]$.

In figure 5, we depict the phase difference and the coherence function W versus $\lg\beta$. The modified decoupling schemes $C_{+1/2}^{\theta^a,-1}C_{-1}^{\theta^c,+1}C_{+1/2}^{\theta^a,-1}$ and $C_{+1/2}^{\theta^a,-1}C_{-1/2}^{\theta^a,+1}C_{-1/2}^{\pi-\theta^a,-1}C_{+1/2}^{\pi-\theta^a,+1}$ suppress the geometric dephasing until $\beta=\Gamma_3T\sim 1$. If the correlation time is less than the evolution time $\beta=\Gamma_3T>1$, any dynamical decoupling schemes fail.

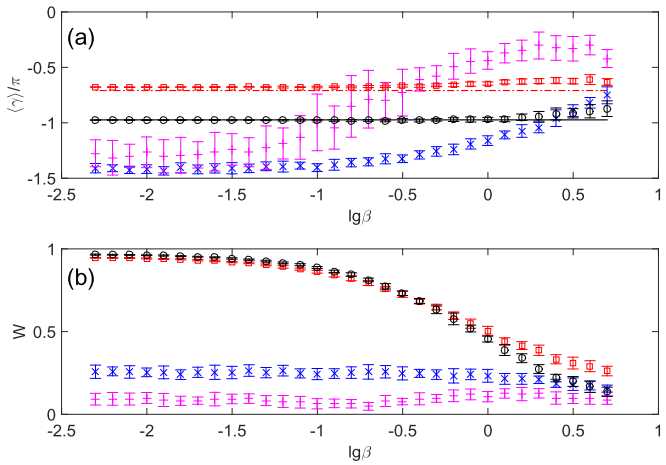

Figure 5. The Berry phase difference $\langle\gamma\rangle$ (a) and coherence function W (b) versus $\beta = \Gamma_3 T$ on the condition of $\theta^a = 5\pi/12$, where all the labels are the same as in figure 4.

Table 1. $h(t,\ T)$ and the corresponding filter functions of several dynamical decoupling sequences.

$h(t,\ T)$	Sequence	$F(z)$
++++	FID	$2\sin^2\frac{z}{2}$
++--	SE	$8\sin^4\frac{z}{4}$
+--+	CPMG ($n=2$)	$8\sin^4\frac{z}{4n}\sin^2\frac{z}{2}\Big/\cos^2\frac{z}{2n}$

5. Discussion and summary

Generally speaking, dephasing is not the only decoherence source in our system when the noise bandwidth Γ_3 becomes large, i.e. $\Gamma_3 \sim B_0$. It induces non-adiabatic transition, which gives the depolarization factor $\exp(-\lambda)$ and the coherence function $W = \exp(-\lambda/2 - \chi)$ [31], where $\lambda = \alpha_3 T \sin^2\theta\Gamma_3/(\Gamma_3^2 + B_0^2)$. In this situation, this kind of strategy of adiabatic driving accompanied by dynamical decoupling sequences does not work.

The foregoing schemes do not involve the case of transverse noise. Recently, the artificial simulated transverse noise with $K_1 = K_r\cos\phi$ and $K_2 = K_r\sin\phi$ has also been studied [25], where K_r is the magnetic field fluctuation in radial direction and it originates from the driving amplitude noise of qubit. Similarly, in the rotating frame, we obtain $\bar{\mathbf{B}}_T = (K_r\cos\theta,\ 0,\ B_0 + K_r\sin\theta)$ and

$$\begin{aligned}\Omega_T &= \left[\left(B_0 - \omega_{\rm rf}\cos\theta + K_r\sin\theta\right)^2 + \left(\omega_{\rm rf}\sin\theta + K_r\cos\theta\right)^2\right]^{\frac{1}{2}} \\ &\approx \Omega + \sin\theta K_r - \frac{\omega_{\rm rf}\cos\theta\sin\theta}{B_0}K_r + o(K_r^2/B_0),\end{aligned} \tag{26}$$

Following the similar procedure discussed in scheme 1, we can also suppress the residual geometric dephasing except θ^a and θ^c satisfy:

$$\sin\theta^a\left(1 - \frac{\omega_B\cos\theta^a}{B_0}\right) = \sin\theta^c\left(1 + \frac{\omega_B\cos\theta^c}{B_0}\right). \tag{27}$$

However, in this situation, the strategy in scheme 2 does not work because $\omega_{\rm rf}\cos\theta$ and $\omega_{\rm rf}\cos\theta\sin\theta/B_0$ have the same sign. In addition, how to design dynamical decoupling sequences that overcome residual geometric dephasing induced by both longitudinal noise and transverse noise simultaneously remains open.

In summary, we have studied how to suppress the geometric dephasing of the Berry phase induced by classical low-frequency fluctuation field $K_3(t)$. By taking advantage of the expansion of the total Hamiltonian in the rotating frame, we analyze the origin of the residual geometric dephasing. In essence, it stems from the time-varying intersection angle between the noise and the effective Hamiltonian related to the rotation direction, which can not be suppressed further by using traditional dynamical decoupling strategies. Furthermore, we

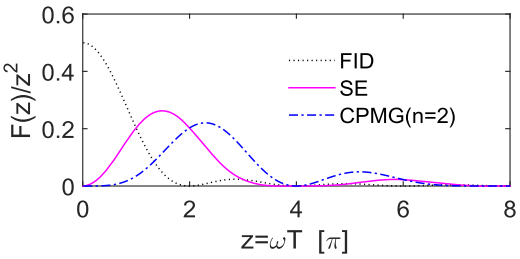

Figure 6. $F(z)/z^2$ versus z for various dynamical decoupling sequences. The frequency with the maximum $F(z)/z^2$ increases as $h(t,\ T)$ switches more times.

present two kinds of modified dynamical decoupling schemes to balance the noises in different time intervals and suppress the residual geometric dephasing. Numerical results verify the validity of our schemes. These schemes will help to generate more high-precision quantum manipulations and to restrain decoherence induced by the low-frequency noise.

Acknowledgments

This work was funded by the National Key Research and Development Program (Grant No.2016YFA0301700), the National Natural Science Foundation of China (Grant No. 11574294, 61490711), and the Strategic Priority Research Program of the Chinese Academy of Sciences (Grant No. XDB01030200).

Appendix. Dynamical decoupling

Dynamical decoupling is used to suppress the low-frequency noise through flipping the coefficients of random noise rapidly. Finally, the random variable in the phase difference is

$$\varphi = \int_0^T h(t,\ T)K_3(t)\mathrm{d}t \tag{A.1}$$

with the function $h(t,\ T) = \pm\ 1$ determined by

$$h(t,\ T) = \sum_{k=0}^{n}(-1)^k\Theta(t_{k+1} - t)\Theta(t - t_k), \tag{A.2}$$

where $\Theta(t)$ is the Heaviside step function, $t_0 = 0$, $t_{n+1} = T$, and n represents the total times of switching between 1 and -1. The time t_k depends on the dynamical decoupling sequences in detail.

Using equation (13), the dephasing is represented by [23]

$$\chi = -\ \ln\ W = \int_0^\infty \frac{\mathrm{d}\omega}{\pi}S_3(\omega)\frac{F(\omega T)}{\omega^2}. \tag{A.3}$$

In table 1, we summarize $h(t,\ T)$ and the corresponding filter functions F of several dynamical decoupling sequences, where $\pm$ refers to the value of the function $h(t,\ T)$ in every time of duration $T/4$. For example, $++++$ refers to $h(t,\ T) = 1$ in the whole time of duration T. Using the spectrum in equation (10), we derive out

$$\chi(T) = \frac{\alpha}{\Gamma_3^2}\begin{cases}\Gamma_3 T - 1 + \mathrm{e}^{-\Gamma_3 T} & \text{FID}\\ \Gamma_3 T - 3 + 4\mathrm{e}^{-\Gamma_3 T/2} - \mathrm{e}^{-\Gamma_3 T} & \text{SE}\\ \Gamma_3 T - 5 + 4\mathrm{e}^{-\Gamma_3 T/4} + 4\mathrm{e}^{-\Gamma_3 T/2} - 4\mathrm{e}^{-3\Gamma_3 T/4} + \mathrm{e}^{-\Gamma_3 T} & \text{CPMG}\ (n = 2)\end{cases} \tag{A.4}$$

Now we analyze the above equation in various limiting cases. For the low-frequency noise, we obtain $\Gamma_3 T \ll 1$. Then equation (A.4) is rewritten as

$$\chi(T) \approx \frac{\alpha T^2}{2}\begin{cases}1 & \text{FID}\\ \Gamma_3 T/6 & \text{SE}\\ \Gamma_3 T/24 & \text{CPMG}(n = 2)\end{cases} \tag{A.5}$$

where the dephasing is suppressed by dynamical decoupling sequences. We plot $F(z)/z^2$ versus z in figure 6, where the low-frequency contribution of noise can be filtered out through some sequences. The frequency with

the maximum $F(z)/z^2$ increases as $h(t,\ T)$ switches more times. For the high-frequency noise with $\Gamma_3 T \gg 1$, $\chi(T) \approx \alpha T/\Gamma_3$ for any sequences, which means that none of them are valid for suppressing the high-frequency noise.

References

[1] Berry M 1984 *P. Roy. Soc. A-Math. Phy.* **392** 45
[2] Jones J A, Vedral V, Ekert A and Castagnoli G 2000 *Nature* **403** 869
[3] Xiao D, Chang M-C and Niu Q 2010 *Rev. Mod. Phys.* **82** 1959
[4] Leek P, Fink J, Blais A, Bianchetti R, Göppl M, Gambetta J, Schuster D, Frunzio L, Schoelkopf R and Wallraff A 2007 *Science* **318** 1889
[5] Ota Y, Goto Y, Kondo Y and Nakahara M 2009 *Phys. Rev.* A **80** 052311
[6] Du J, Zou P, Shi M, Kwek L C, Pan J-W, Oh C H, Ekert A, Oi D K and Ericsson M 2003 *Phys. Rev. Lett.* **91** 100403
[7] Filipp S, Klepp J, Hasegawa Y, Plonka-Spehr C, Schmidt U, Geltenbort P and Rauch H 2009 *Phys. Rev. Lett.* **102** 030404
[8] Zhang Y, Tan Y-W, Stormer H L and Kim P 2005 *Nature* **438** 201
[9] Falci G, Fazio R, Palma G M, Siewert J and Vedral V 2000 *Nature* **407** 355
[10] Falci G, Fazio R and Palma G M 2003 *Fortschr. Phys.* **51** 442
[11] Aharonov Y and Anandan J 1987 *Phys. Rev. Lett.* **58** 1593
[12] Carollo A, Fuentes-Guridi I, Santos M F and Vedral V 2003 *Phys. Rev. Lett.* **90** 160402
[13] Tong D, Sjöqvist E, Kwek L C and Oh C 2004 *Phys. Rev. Lett.* **93** 080405
[14] Shnirman A, Makhlin Y and Schön G 2002 *Phys. Scripta* **2002** 147
[15] Chirolli L and Burkard G 2008 *Adv. Phys.* **57** 225
[16] Preskill J 1998 *P. Roy. Soc. A-Math. Phy.* **454** 469
[17] Koh T S, Gamble J K, Friesen M, Eriksson M and Coppersmith S 2012 *Phys. Rev. Lett.* **109** 250503
[18] Solinas P, Zanardi P and Zanghí N 2004 *Phys. Rev.* A **70** 042316
[19] Leibfried D, DeMarco B, Meyer V, Lucas D, Barrett M, Britton J, Itano W, Jelenković B, Langer C and Wineland D J 2003 *Nature* **422** 412
[20] Blais A and Tremblay A-M 2003 *Phys. Rev.* A **67** 012308
[21] De Chiara G and Palma G M 2003 *Phys. Rev. Lett.* **91** 090404
[22] Bylander J, Gustavsson S, Yan F, Yoshihara F, Harrabi K, Fitch G, Cory D G, Nakamura Y, Tsai J-S and Oliver W D 2011 *Nat. Phys.* **7** 565
[23] Cywiński Ł, Lutchyn R M, Nave C P and Sarma S D 2008 *Phys. Rev.* B **77** 174509
[24] Berger S, Pechal M, Abdumalikov A Jr, Eichler C, Steffen L, Fedorov A, Wallraff A and Filipp S 2013 *Phys. Rev.* A **87** 060303
[25] Berger S, Pechal M, Kurpiers P, Abdumalikov A, Eichler C, Mlynek J, Shnirman A, Gefen Y, Wallraff A and Filipp S 2015 *Nat. Commun.* **6** 8757
[26] Whitney R S 2010 *Phys. Rev.* A **81** 032108
[27] Whitney R S, Makhlin Y, Shnirman A and Gefen Y 2005 *Phys. Rev. Lett.* **94** 070407
[28] Bergli J, Galperin Y M and Altshuler B 2009 *New J. Phys.* **11** 025002
[29] Charlebois D, Exact numerical simulation of the ornstein-uhlenbeck process (http://mathworks.com/matlabcentral/fileexchange)
[30] Gillespie D T 1996 *Phys. Rev.* E **54** 2084
[31] Ithier G *et al* 2005 *Phys. Rev.* B **72** 134519